Vehicle/Atmosphere Interaction Glows: Far Ultraviolet, Visible, and Infrared

G. Swenson
University of Illinois, Urbana, Illinois

October 1999

The NASA STI Program Office...in Profile

Since its founding, NASA has been dedicated to the advancement of aeronautics and space science. The NASA Scientific and Technical Information (STI) Program Office plays a key part in helping NASA maintain this important role.

The NASA STI Program Office is operated by Langley Research Center, the lead center for NASA's scientific and technical information. The NASA STI Program Office provides access to the NASA STI Database, the largest collection of aeronautical and space science STI in the world. The Program Office is also NASA's institutional mechanism for disseminating the results of its research and development activities. These results are published by NASA in the NASA STI Report Series, which includes the following report types:

- TECHNICAL PUBLICATION. Reports of completed research or a major significant phase of research that present the results of NASA programs and include extensive data or theoretical analysis. Includes compilations of significant scientific and technical data and information deemed to be of continuing reference value. NASA's counterpart of peer-reviewed formal professional papers but has less stringent limitations on manuscript length and extent of graphic presentations.

- TECHNICAL MEMORANDUM. Scientific and technical findings that are preliminary or of specialized interest, e.g., quick release reports, working papers, and bibliographies that contain minimal annotation. Does not contain extensive analysis.

- CONTRACTOR REPORT. Scientific and technical findings by NASA-sponsored contractors and grantees.

- CONFERENCE PUBLICATION. Collected papers from scientific and technical conferences, symposia, seminars, or other meetings sponsored or cosponsored by NASA.

- SPECIAL PUBLICATION. Scientific, technical, or historical information from NASA programs, projects, and mission, often concerned with subjects having substantial public interest.

- TECHNICAL TRANSLATION. English-language translations of foreign scientific and technical material pertinent to NASA's mission.

Specialized services that complement the STI Program Office's diverse offerings include creating custom thesauri, building customized databases, organizing and publishing research results...even providing videos.

For more information about the NASA STI Program Office, see the following:

- Access the NASA STI Program Home Page at *http://www.sti.nasa.gov*

- E-mail your question via the Internet to help@sti.nasa.gov

- Fax your question to the NASA Access Help Desk at (301) 621–0134

- Telephone the NASA Access Help Desk at (301) 621–0390

- Write to:
  NASA Access Help Desk
  NASA Center for AeroSpace Information
  7121 Standard Drive
  Hanover, MD 21076–1320

Vehicle/Atmosphere Interaction Glows: Far Ultraviolet, Visible, and Infrared

G. Swenson
University of Illinois, Urbana, Illinois

National Aeronautics and
Space Administration

Marshall Space Flight Center • MSFC, Alabama 35812

October 1999

TABLE OF CONTENTS

LIST OF FIGURES

LIST OF FIGURES (Continued)

LIST OF TABLES

LIST OF ACRONYMS

AE	Atmospheric Explorer
AO	atomic oxygen
CMG	control moment gyro
DE	Dynamic Explorer
EISG	Experimental Investigation of Spacecraft Glow
FUV	far ultraviolet
H	hydrogen
H_2O	water
IDL	interactive digital language
IR	infrared
IRT	infrared telescope
ISO	Infrared Space Observatory
LBH	Lyman-Birge-Hopfield
LEO	low-Earth orbit
LESC	Lockheed Engineering and Systems Company
LPARL	Lockheed Palo Alto Research Laboratory
MPESS	mission peculiar experiment support structure
MSFC	Marshall Space Flight Center
N	nitrogen
Ni	nickel
NO	nitric oxide
NO_2	nitrogen oxide
O	oxygen
OAST	Office of Astronautics and Space Technology
OMS	orbital maneuvering system
RMS	remote manipulator system
SEE	Space Environmental Effects
UV	ultraviolet

CONTRACTOR REPORT

VEHICLE/ATMOSPHERE INTERACTION GLOWS:
FAR ULTRAVIOLET AND INFRARED

1. INTRODUCTION

Spacecraft glow studies have been performed with the Experimental Investigation of Spacecraft Glow (EISG), which flew on Space Transportation System (STS)–62 as part of the Office of Astronautics and Space Technology (OAST) payload. The experiment flew as a Hitchhiker payload. Glow studies have been done since they were discovered on STS–3, as crewmen viewed the phenomena from the aft flight deck. Film pictures documented the early observed phenomena, as exemplified in figure 1.

Figure 1. An image of Shuttle glow taken on STS–8. The orange
glow is observed to extend away from the surface—an early
emission mystery.

The EISG payload consisted of visible, ultraviolet (UV) and far ultraviolet (FUV), and infrared (IR) instrumentation. A schematic of the payload is shown in figure 2, and a picture of the instrument integration nearing its completion is shown in figure 3. The instrumentation was built and assembled by a team managed from the Lockheed Palo Alto Research Laboratory (LPARL) but engineered with both LPARL and the Lockheed Engineering and Systems Company (LESC), Houston, TX. The NASA management of the experiment was provided by the materials group at NASA Johnson Space Center and the payload integration and operations support was performed by the Hitchhiker office at NASA Goddard Space Flight Center. It was truly a well chosen path for the payload system as engineering and support groups from both NASA and Lockheed worked as a team to accomplish the successful development and mission, achieving most of the objectives set initially.
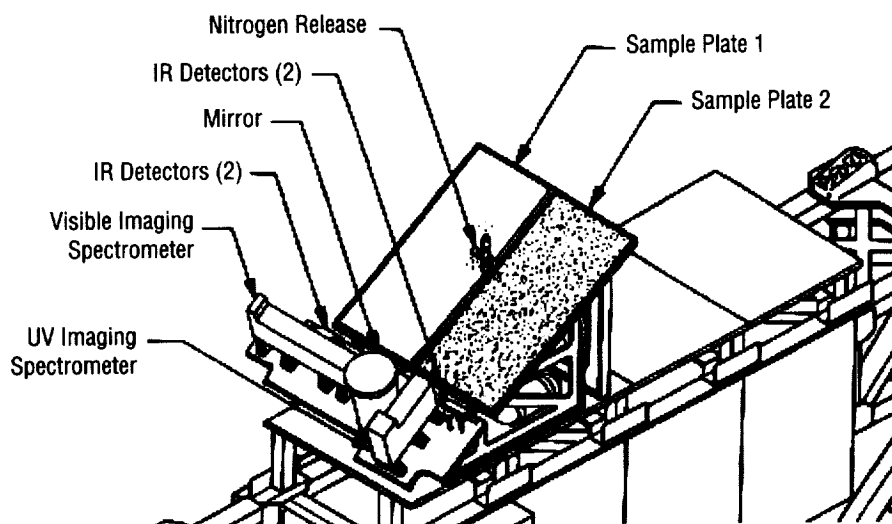
Figure 2. Schematic describing the EISG, which participated in the STS–62 mission, shown integrated to the Hitchhiker bridge structure. The optical detectors viewed into a mirror which in turn directed the viewing fields over two material samples. The left sample was a white Chemglaze™ (A276) and the right, a black carbon paint (Z306).

Figure 3. The integrated EISG experiment. Note gas release nozzles protruding above the samples which directed gas both outward and downward onto the surfaces.

On orbit, the integrated payload can be seen from the aft flight deck camera on the orbiter (fig. 4) and from the wrist camera on the remote manipulator system (RMS) (fig. 5). The wrist camera complemented the observations as the view along the plate clearly showed ram glow on the sample plate (fig. 6). The classical experiment to test atom exchange with molecular nitrogen (N) was performed with a gas release which released the plum on and in front of the sample plate. The experiment proved that molecular N did not atom exchange at the orbital velocity. In fact, the gas cloud sufficiently attenuated the ram oxygen (O) beam (and energy) which resulted in extinguishing the glow (fig. 7).

Figure 4. The payload bay from the aft flight deck near sunrise on STS–62. A glint of sunlight is seen on the orbiter bay. Glows can also be seen on the port side the vertical stabilizer and the starboard orbital maneuvering system (OMS) pod. The EISG payload is visible on the mission peculiar experiment support structure (MPESS) in the lower left with the logo on the insulation blanket.

Figure 5.   A view of the EISG experiment in the payload bay during an orbital daytime.
The orbiter RMS wrist camera is being used to make the observation
along the normal to the sample plate.
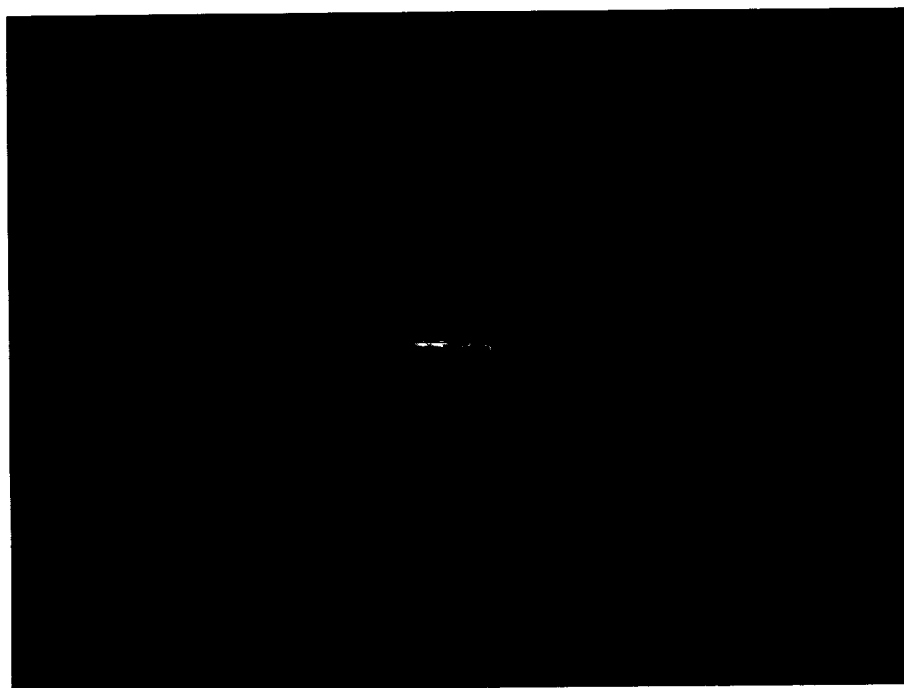
Figure 6.   An orbital nighttime image from the same camera with the same viewing
geometry as figure 5. Note the glow on the sample plate.

4
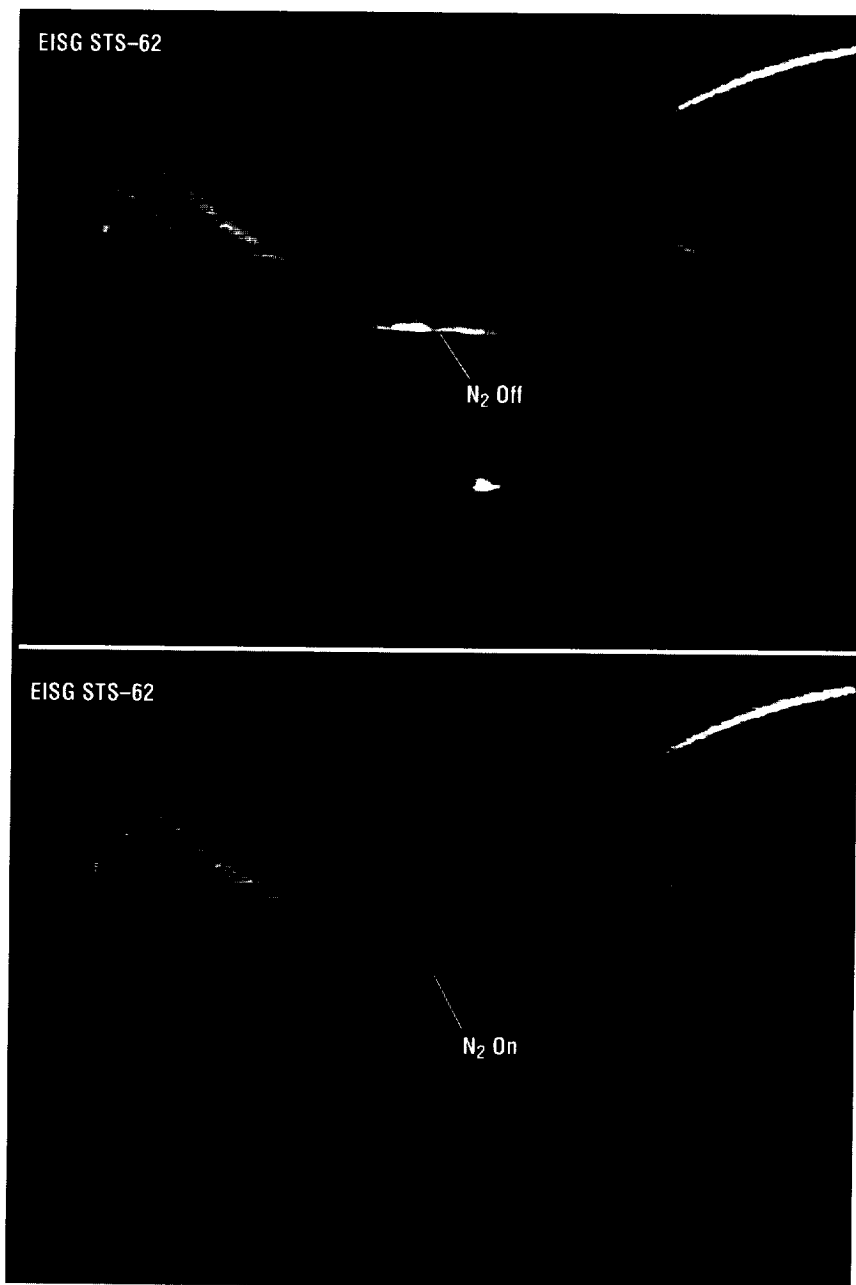
Figure 7. The same view as shown in figures 5 and 6. The glow visible on the sample plate in the top image is extinguished during the N_2 gas release in the bottom panel. This is due to the release gas becoming collisionally thick to the ramming O, and consequently, reducing the fluence and O velocity (and energy) necessary for the heterogeneous chemistry to take place which normally leads to the glow reaction.

This data analysis task has been supported by the Space Environmental Effects (SEE) program and managed from the materials group at the NASA Marshall Space Flight Center (MSFC). This study evolved models of the visible, FUV, and IR glows for engineering replication of glow processes. The models and suggested mitigation are contained in this report.

2. VISIBLE REGION

Visible glow has been reported on ram surfaces of the Atmospheric Explorer–E (AE), Dynamic Explorer–B (DE).[1-4] The spectral observations from the AE and Space Shuttle suggest a "red" glow, although the course spectral shape is not the same for the two spacecraft. The AE and DE data support an O intensity dependence with altitude. This O dependence is qualitatively supported in the STS observations as well. The major difference between the two would appear to be the surface e-fold of the emission, determined to be 20 cm by Yee and Abreu[2] and verified by Swenson et al.[5] for the STS observations. The ram angle effect of the AE glow appears to closely follow a cosine relationship with the ram angle. The ram angle of the stabilizer seems to produce slightly more glow at high ram angles than the cosine effect, yet an unexplained phenomenon.

It was later found from the STS database that the intensity for similar altitudes showed significant differences in brightness. Analysis has revealed that the rammed surface temperatures were significantly different for these measurements.[6] Subsequent analysis uncovered an explanation which is consistent with an earlier theory that supports the fact that nitric oxide (NO) is held in bond on the surface for ramming O atoms to form nitrogen oxide (NO_2) in three-body recombination, where the NO_2 vibrationally relaxes to produce the glow. It was also suggested that the 0.14-eV bond energy of the NO would be consistent with the lesser intensity seen on the AE spacecraft since the AE spacecraft surface was much warmer than the STS tile surfaces[6]. Yee et al.[4] suggested that a portion of the AE glow was also likely a result of NO_2 emission.

An analytical glow intensity model has been developed to fit the experimental results by Swenson and Mende[7] which was later refined by Swenson and Rairden.[8] This model assumes a cosine ram angle dependence, an O scale height dependence, and a surface temperature dependence. The validity of the model in the spectral range (4,000–8,000 Å) is supported by the good fit of the model to the observed slit spectral intensity flown on board the STS–41–D[9] and STS–62.[10,11]

The model takes the form:

$$I_{x,\phi,T,\lambda} = 0.084 \cdot \frac{O_z}{O_{250}} \cos(\phi_r) \cdot e^{930/T_s} \cdot \cos(0.0005 \cdot |6,800 - \lambda|)^3 \ , \tag{1}$$

where

$I_{x,\phi,T,\lambda}$ = intensity, Rayleigh/Angstrom
O_z = atomic oxygen (AO) density at altitude, z
O_{250} = AO density at 250 km
ϕ_r = the angle that a surface makes with ram, degree (0–90)
T_s = surface temperature, K (190–450)
λ = wavelength, Angstrom (4,000–8,000).

An example of the model output may be found in figure 8. The assumptions were a surface temperature of 300 K, ram angle of 45°, and altitude of 400 km.

6

2.1 Use of the Model

The model is coded in interactive digital language (IDL) with the following input and output parameters:

Input parameter:

> t_surf: surface temperature, 190–450 K
> ram_angle: ram angle of the Shuttle position, 0°–90°
> Altitude: altitude of the Space Shuttle

Output parameter:

> Wavelength: wavelength of the investigation
> Intensity: spectral intensity of the surface glow.

The altitude dependence is calculated as the ratio of AO intensity at altitude z and at 250 km. AO intensity between 200–600 km with 20-km increments was derived using MSIS86 model[12] using a set of default input parameters. Users can run the MSIS86 model using the parameters other than the default values to get the dependence for their special case.

To run the program, type ".run model_vs" at the IDL prompt and type the input parameters in response to the prompts. The resulted model will be plotted on the screen. The output parameters will be written into an ASCII file named "output.txt". The output figure can also be plotted to a postscript file and printed to a postscript printer using the switch flag. A model result for the indicated conditions is shown in figure 8.

Enhanced visible glows 557.7- and 630-nm observed due to NO products from hydrazine doping of surfaces.[13] Enhanced O 557.7- and 630-nm emissions were also observed.[14] Visible spectral enhancements due to thrusters have not been modeled here.
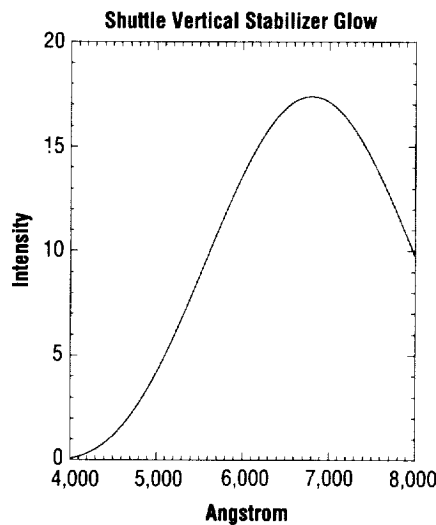

Figure 8. A model output of the visible glow for the following conditions: surface temperature = 220 K, ram angle = 10°, and altitude = 300 km. The glow is due to surface recombination which leads to NO_2 emission.

3. ULTRAVIOLET REGION

Historically, UV and FUV emissions have been observed on a number of spacecraft. UV glows were reported in the 2,800 and 3,371 Å channels of the AE spacecraft.[1,2] The UV glows were considerably weaker than glows in visible wavelengths on that spacecraft. It is assumed that the UV glows from NO might likely be on ram surfaces.[5,6,15–17] Kofsky[18] and Swenson and Meyerott[19] have proposed recombination of N on the surface as being responsible. Swenson and Meyerott[19] have found that a large source of N is likely in the plow cloud of low-altitude spacecraft due to atom exchange with the ramming atmosphere. This mechanism predicts a source flux and altitude distribution that supports the observations. Meyerott and Swenson[20,21] have described a set of possible surface interactions likely with fast N recombination, including the possibility of 958 Å and 2,800–3,400 Å (Gaydon-Herman bands) from excited N recombination. Meyerott and Swenson[21] presented a chemical explanation for fast recombination of N which would result in an N_2 upper state that would cascade to produce a source of N_2 Lyman-Birge-Hopfield (LBH) bands as observed by Torr and Torr.[22] Hunton[13] and Hunton and Machuzak[23] have verified the production of N and NO products in O-bombarded thruster plumes.

The EISG was flown on STS–62 in March, 1994.[8,10] Many spectra were recorded by an FUV spectrometer that confirmed the existence of the UV and FUV surface glow.[24] The major bright glow appeared to be of sporadic nature in the 2,200–3,000 Å spectral region. In particular, in the middle grating position the FUV channel displayed sporadic anomalous emission in the decent portion of the EISG 6 and 7 elliptical orbits when the Space Shuttle took the position where the sample plate was directed into ram. This sporadic emission featured a concentration of emission of energy in the short wavelength range between 2,200 and 3,000 Å. In the laboratory experiment, a fast O beam was directed into the N_2 and a sample plate to simulate the ram fluence. The primary emission of the lab glow is NO. The STS–62 and laboratory measured spectra, and the NO band heads are shown in figure 9. Laboratory results of similar experiments with IR measurements have been reported by Upschulte et al.[25] The similarity between lab and ram glow indicates that the spectral bands emitting are the same but the vehicle glow relative to the laboratory observation was a rotationally hot emission, likely due to the extremely high recombination temperature.

These constituents that produce the UV surface glow can be scavenged from the atmosphere. In addition, monomethyl hydrazine thruster effluents interacting with the atmosphere are observed to produce large amounts of N and NO, likely through O collisions with exhaust products of vibrationally enhanced molecular N. These products produce both gas phase and surface (heterogeneous) reactions, resulting in UV and FUV glows.
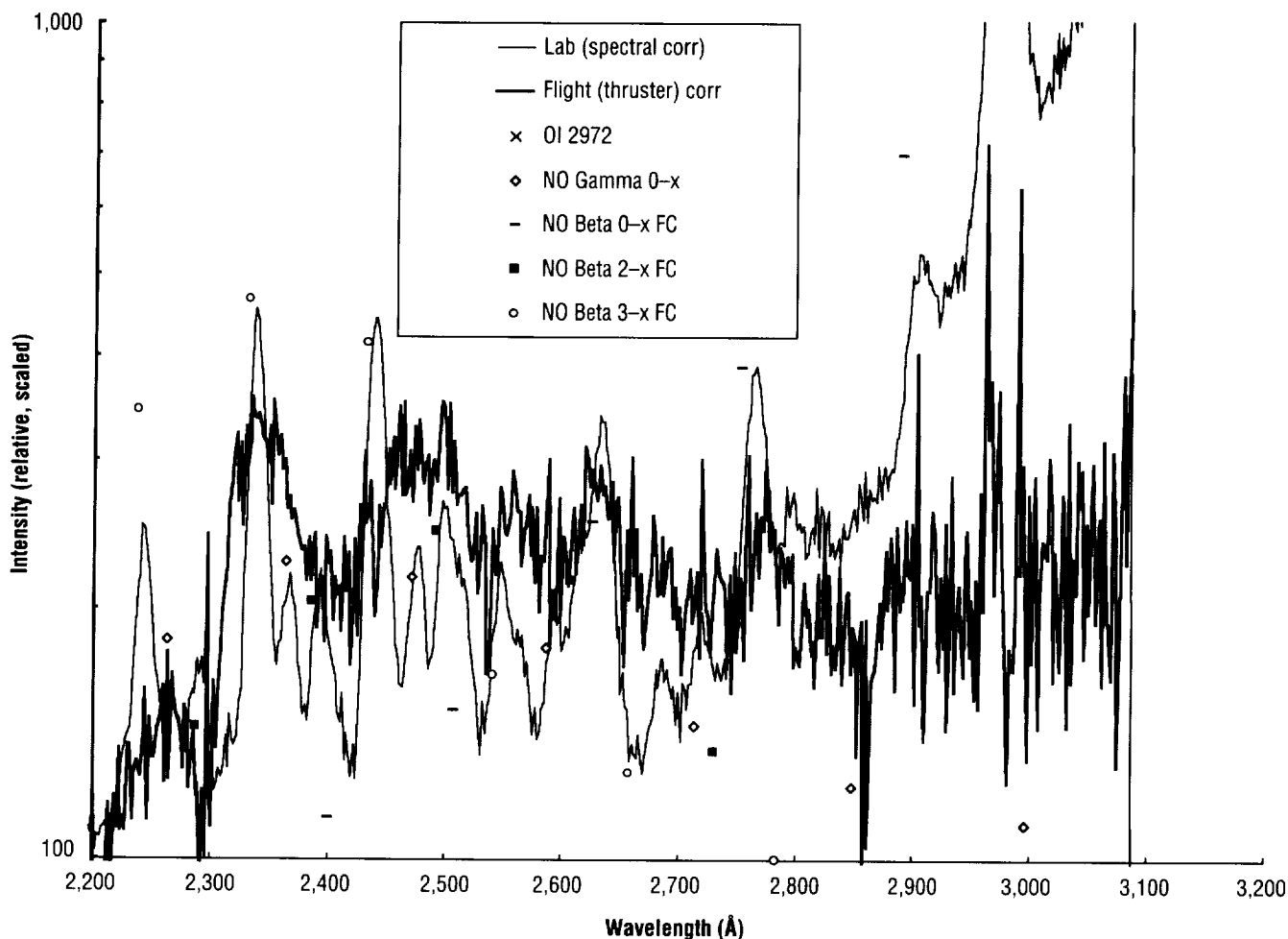
Figure 9.   A plot of FUV data and model information. The heavy line is the flight spectrum of FUV glow subsequent to thruster effluent doping of the EISG surface. The thin line is a spectrum taken with the same instrument of a laboratory experiment. The dots describe NO γ and β bandheads which are shown to correspond to the intensity peaks in the spectra. The flight spectra is "filled in" due to the effective high temperature of the on-orbit chemistry.

3.1 Computer Simulation of the Ultraviolet Surface Glow

To further investigate mechanisms of vehicle glow, a spectral model has been developed. The spectral model is based on the assumption that the vehicle glow is mainly from the emission of the NO β, δ, and γ bands. For the vibrational band, the wave number of the spectrum is given by Herzburg,[26]

$$v = v + \omega'_e(v' + 1/2) - \omega'_e x'_e(v' + 1/2)^2$$

$$+\omega'_e y'_e(v' + 1/2)^3 + \ldots - [\omega''_e(v'' + 1/2)$$

$$-\omega''_e x''_e(v'' + 1/2)^2 + \omega''_e x''_y(v'' + 1/2)^3 + \ldots] \cdot \tag{2}$$

The coefficients were given by Herzberg[26] in the form of a table. Tanaka[27] found that in the NO afterglow the emission intensity is about the same for β, δ, and γ bands systems. Therefore, in our model spectrum the weights for β, δ, and γ bands are taken to be equal. The magnitude of the composite spectrum is normalized to the measured spectrum. According to Gaydon,[28] the emission intensity from the higher vibrational state of the band is weaker. However, in our simulation we still include the higher vibrational transitions because the theoretical calculation shows emission from some higher vibrational transitions cannot be ignored. In fact, we included in our model up to quantum number 23 and to the upper energy level 15 for γ, 19 for β, and 5 for δ bands.

3.2 Running the Programs

A FORTRAN90 program "synth_new.f" calculates the bandhead positions for γ, β, and δ bands and uses these calculated bandhead positions to simulate the laboratory and the spacecraft surface NO glow spectrum. The compilation command on the IBM J40 is "xlf90 synth_new f". (This command will vary according to different venders). To run the program after compilation, type "a.out". The calculated bandhead positions are written into the file "gamma_band_position.txt", "beta_band_position.txt", and "delta_band_position.txt" for γ, β, and δ bands, respectfully. The simulated laboratory and spacecraft NO glow spectral intensities and the corresponding wavelengths are written into the files named "lab_simulation.txt" and "space_simulation.txt" in response to user choice. For comparison, the experimental spectral data are also written to this file.

Since the FORTRAN program cannot provide the graphic function, an IDL program "f_rslt.pro" is used to plot the spectrum. The synthetic spectrum was composed as a summation of the triangle pulses centered at each position with the pulse width of half of the input spectral resolution. The spectral magnitude of the model is scaled to the measured spectra from the STS–62 mission. Intensity in Rayleigh/Angstrom is plotted versus wavelength. An example output is shown in figure 10, along with an overlay of the flight spectra which was previously shown in figure 9 as it was compared with the laboratory-generated spectra formed by an O beam flowing onto a plate with NO doping.
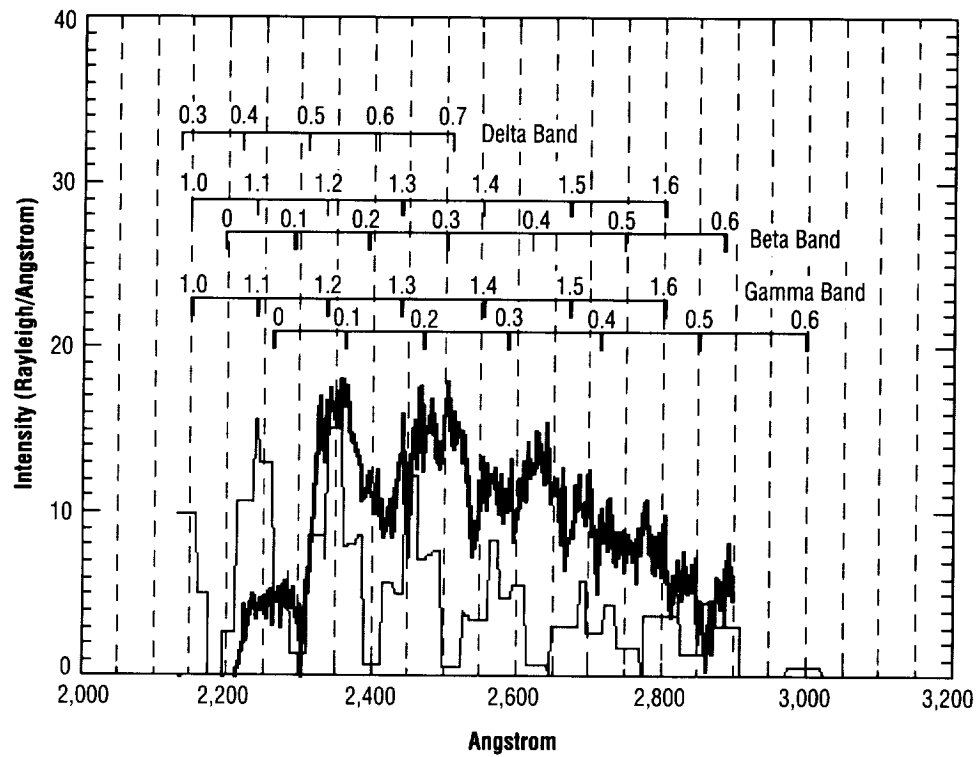
10

Figure 10. Example output of intensity in Rayleigh/Angstrom versus wavelength. Also, an overlay comparison of flight spectra.

11

4. INFRARED REGION

The data from the infrared telescope (IRT), flown on STS–51–F Spacelab 2 mission, were originally reported by Koch et al.[29] as originating from near orbital emissions, primarily water (H_2O). IR measurements were made in the 1.7–3, 4.5–9.5, 6.1–7.1, and 8.5–14.5 μm bands. These observations were made close to perpendicular to the velocity vector and interpreted as being solely due to excited H_2O vapor. The excitation is caused by solar and Earth shine radiation and by collisions with ambient AO. The outgassing molecules travel with the spacecraft at $\approx$7.75 km/sec which, when combined with a thermal velocity of the O atoms at $\approx$1,000 K, correspond to a relative translation energy (RTE) between 1.93 and 3.51 eV. The signal in the 1.7- to 3-μm band was observed to change each time the spacecraft passed through the terminator. Since the radiation excitation cross section and solar flux are known, these data provide a measure of the H_2O column density. This combined data were then used to provide information on the collisional excitation cross sections of the low-lying vibrational levels of H_2O by AO at an RTE of $\approx$3 eV. The IRT data for the 4.5- to 9.5-μm sensor and the nighttime data for the 1.7- to 3-μm sensor are consistent with theoretical collisional excitation of H_2O by AO. Diurnal variations of 4.5- to 9.5-μm intensities follow the model-predicted O density for a full orbit. Cross sections for the collisional excitation process were derived by Meyerott et al.[30]

4.1 Theoretical Simulation

Theoretical spectra of H_2O vapor for the lowest vibrational/rotational v_1 (100)$\rightarrow$(000), v_2 (010) $\rightarrow$(000), and v_3 (001)$\rightarrow$(000) bands have been produced with Briss' algorithm[30] as part of the investigation of the collisional excitation of the outgassing H_2O by Orbital $O(^3P)$ in the Space Shuttle environment.

4.2 Briss' Algorithm

Briss' algorithm allows the calculation of the line position and the relative line intensity of an asymmetric molecule once the Watson-type hamiltonian[32] is given. The hamiltonian includes the quartic and sextic centrifugal distortions and takes the following form:

$$H = A_k J_z^2 + A_j J^2 + \tfrac{1}{2}a(J_+^2 + J_-^2) - D_k J_z^4 - D_{jk}J^2 J_z^2 - D_j J^4 - \tfrac{1}{2}[d_k J_z^2 + d_j J^2, J_+^2 + J_-^2]_+$$

$$+H_k J_z^6 + H_{kj}J^2 J_z^4 + H_{jk}J^4 J_z^2 + H_j J^6 + \tfrac{1}{2}[h_k J_z^4 + h_{jk}J^2 J_z^2 + h_j J^4, J_+^2 + J_-^2]_+ \quad , \qquad (3)$$

where $[A, B]_+$ represents the anticommunicator, and $[A, B]_+=AB+BA$. The coefficients of the hamiltonian are determined by the least-square fit to the high-precision experimental spectra. The hamiltonian is in the base of the symmetry adapted symmetric rotor function,

$$|J,K,\pm,m\rangle = \{(|J,K,m\rangle \pm |J,-K,m\rangle\}/\sqrt{2}, \qquad |J,0,+,m\rangle = |J,0,m\rangle \quad . \qquad (4)$$

The matrix elements in this base are given by Briss.[28] By construction of the matrix of the hamiltonian and conducting the matrix diagonalization, the eigenvalues of the hamiltonian operator can be obtained, hence the energy levels of the molecule. The algorithm further uses the symmetry transformation to obtain the eigenvectors of the hamiltonian operator and uses them to calculate the relative line intensities.

4.3 The Model of a Water Molecule

An H_2O molecule is a highly asymmetric top molecule with the moments of inertia (in 10^{-40} gm cm^2) at equilibrium position I_a=1.0243, I_b=1.9207, and I_c=2.9470. The geometrical parameters of the molecule were determined from an analysis of the rotational structure of IR bands and by microwave spectroscopy:

$$R(O-H)=0.9572\pm0.003 \text{ Å}; \quad \angle HOH = 104°31'\pm3' \ . \tag{5}$$

The geographical configuration and the axes of the moments of inertia are shown in figure 11. This geometric configuration falls into the C_{2v} group. The symmetry species of the dipole moment components μ_a, μ_b, μ_c, direction cosines λ_{Za}, λ_{Zb}, λ_{Zc}, normal coordinates Q_k (k=1, 2, and 3) and the rotational wave functions $|J_{KaKc}\rangle$ of the H_2O molecule in the C_{2v} group are given in table 1.
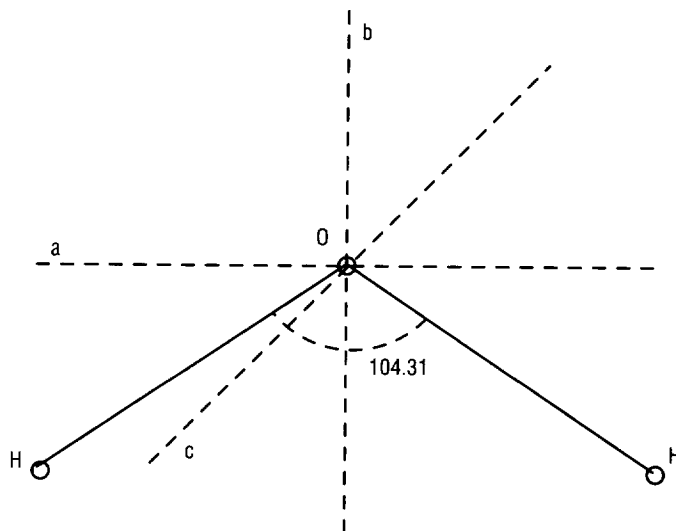
Figure 11. Geographic configuration and the axes of the moments of inertia.

Table 1. Symmetry species that determine the selection rules of the transitions.

Quality	Species	Quality	Species
μ_a	B_2	Q_1, Q_2	A_1
μ_c	A_1	Q_3	B_2
μ_c	B_1	ee	A_1
λ_{Za}	B_1	oo	A_2
λ_{Zb}	A_2	eo	B_1
λ_{Zc}	B_2	oe	B_2

The symmetry characteristics solely determine the selection rules for the IR transitions. The allowed transitions are either the μ_b type (B bands, between vibrational states of the same symmetry species) or of the μ_a type (A bands, between vibrational states of the A_1 and B_2 species). Allowed rotational transitions in the B-type bands are ee↔oo and eo↔oe. In A-type bands, the allowed rotational transitions are ee↔eo and oo↔oe.

In the H_2O molecule, exchanging of the nuclei of the two hydrogen (H) atoms leads to two different wave functions—the symmetric and antisymmetric. The nuclear spin of the H atom is I=_. The total nuclear spin T of H_2O molecules are different—one for antisymmetric and zero for symmetric. According to the general discussion of the angular momentum, a system with a total spin T has $2T+1$ degenerate state in the situation when there is no magnetic filed. Therefore, the antisymmetric rotational levels occur three times as frequently as the symmetric. As a result, the intensity of the transition is weighed differently—one for symmetric and three for antisymmetric.

4.4 Determination of the Relative Population Density

The intensity of a spectral line is give by Briss:[31]

$$I = C(T)g_i e^{-E_i/kT}(1-e^{-hv/kT})|\ i'|\mu|i\ |^2\ ,$$

(6)

in which $C(T)$ is a constant containing the temperature-dependent partition function and v is the frequency of the transition from the upper to the lower state. Factor g_i corresponds to the nuclear statistical weight. Boltzman distribution is assumed whenever the temperature K is input.

The H_2O vapor in the Spacelab environment cannot be treated as equilibrium because the excitation is due to the collision with O atoms that are moving toward the Spacelab with a velocity ≈7.8 km/sec; that is, far greater than the speed of the random thermal motion of the H_2O molecules. Redmon et al.[33] calculated the cross section for vibrational excitation in $O(^3P)$ + $H_2O(000)$ using the quasi-classical method. They also give the final distribution of the cross sections for the pure rotation excitation (000) →(000), and the cross sections for the v_1 (100)→(000), v_2 (010)→(000), and v_3 (001)→(000) bands. The theoretical results of the cross section for the (100) band was in reasonable agreement with the experimental shock tube results. The (010) excitation cross section is larger than the corresponding experimental results. Nevertheless, results from Redmon et al.[33] give us the rough estimation of the probability of the H_2O molecules to be excited to a particular energy level due to the collision with the orbital O atoms. Furthermore, since we do not have enough information to estimate the relative population at different energy levels, we simply use the final rotational distribution given by Redmon et al.[33] to calculate the line intensity.

4.5 Input Parameters

An important issue in producing H_2O emission spectra is to find out the collection coefficients to build up the hamiltonian for different energy levels for H_2O molecules. There are 15 coefficients in the hamiltonian operator. The coefficients used were for the (000) and (010) band published by Camy-Peyret and Flaud[34] and the coefficients for (100) and (001) bands published by Flaud and Camy-Peyret.[35] In their works, the interaction between different states was considered so that the hamiltonian contains

14

terms higher than the sextic order. To fit Briss' algorithm, the higher order was simply truncated and coefficients up to the sextic order were used. Since some of the coefficients in the higher order were comparable with that for the sextic order, it unavoidably introduced some inaccuracies.

The coefficients and some parameters are summarized in table 2.

Table 2. Parameters for the hamiltonian for different energy levels: A_k=A–(B+C)/2, A_j=(B+C)/2, a=(B–C)/2.

Coefficient and Parameters	(000)	v_1 (100)	v_2 (010)	v_3 (001)
Band Origin (cm⁻¹)	0.0	3652.474	1594.74498	3755.92948
Band Type	2 (B type)	1 (A type)	2 (B type)	1 (A type)
A	27.880678	27.12217	31.12835	26.64805
B	14.521689	14.30477	14.687569	14.431302
C	9.277459	9.10457	9.129132	9.138167
D_k	0.32519900D–01	0.30230000D–1	0.57556400D–01	0.25584000D–1
D_{jk}	–0.57655000D–02	–0.5384700D–2	–0.76053000D–02	–0.5656100D–2
D_j	0.12489400D–02	1.23300000D–3	0.13953700D–02	1.30549000D–3
d_k	0.13007000D–02	1.24050000D–3	0.37662000D–02	1.32610000D–3
d_j	0.50838000D–03	4.99870000D–4	0.57879000D–03	5.38170000D–4
H_k	0.12281000D–03	1.00160000D–4	0.35347600D–03	0.84070000D–4
H_{kj}	–0.13700000D–04	–1.4180000D–5	–0.44954000D–04	–1.4992000D–5
H_{jk}	–0.19210000D–05	0.0	0.28820000D–05	0.0
H_j	0.45061000D–06	4.40200000D–7	0.61180000D–06	6.02200000D–7
h_k	0.47916000D–04	0.43320000D–4	1.68526000D–3	0.45320000D–4
h_{jk}	–0.84200000D–06	0.0	0.0	2.13000000D–6
h_j	0.451320000D–06	4.66200000D–7	0.58234000D–6	6.17400000D–7

Other parameters:
Reduction indicator   1
Representation indicator   1
Nuclear indicator (ee, eo, oo, oe) 1, 3, 1, 3

4.6 Program Operation

This FORTRAN program calculates the theoretical spectra of H_2O vapor for the rotational and the lowest vibrational/rotational (100)–(000), (010)–(000), and (001)–(000) bands using the Briss algorithm.[31]

The spectrum of the collisional excitation of the outgassing H_2O by orbital $O(^3P)$ is simulated by including the distribution of the cross sections for the pure rotation excitation (000)–(000), and the cross sections for the (100)–(000), (010)–(000), and (001)–(000) bands given by Redmon et al.[33]

This program can also produce the H_2O vibrational/rotational spectrum for the thermal equilibrium, assuming that the Boltzmann distribution stands.

The program read input file to get the coefficients of the hamiltonian is "input0-0, input1-0, input2-0, and input3-0". It also reads file "phs7.input" for the output control. The output files are OUTPUT0, OUTPUT1, OUTPUT2, OUTPUT3, and SYNTH, which contain the spectral intensity for the pure rotational band, the three lowest vibrational/rotational bands, and the composite band, respectfully.

The procedure to compile and execute the program is as follows:

- Move Asyrot.f, interface.f, input0_0, input1-0, input2-0, input3_0,
  and phs7.input to the same directory
- Compile the source programs using command "f77 *.f"
- Execute the executable file a.out
- Plot the desired spectrum using included IDL program.

4.7 Water Vapor Emission Spectra

Theoretical H_2O vapor spectra are shown in figure 12 for pure rotational band (000)→(000), v_1 (100)→(000) (fig. 13), v_2 (010) →(000) (fig. 14), and v_3 (001)→(000) (fig. 15), respectively. These spectra are the simulations of the emission of H_2O vapor excited by collision with O atoms in the orbital Space Shuttle environments. Each plot has 501 data points with a data interval of 11.9 cm^{-1}. A composite of these theoretical spectra is shown in figure 16.

16

Rotational Band
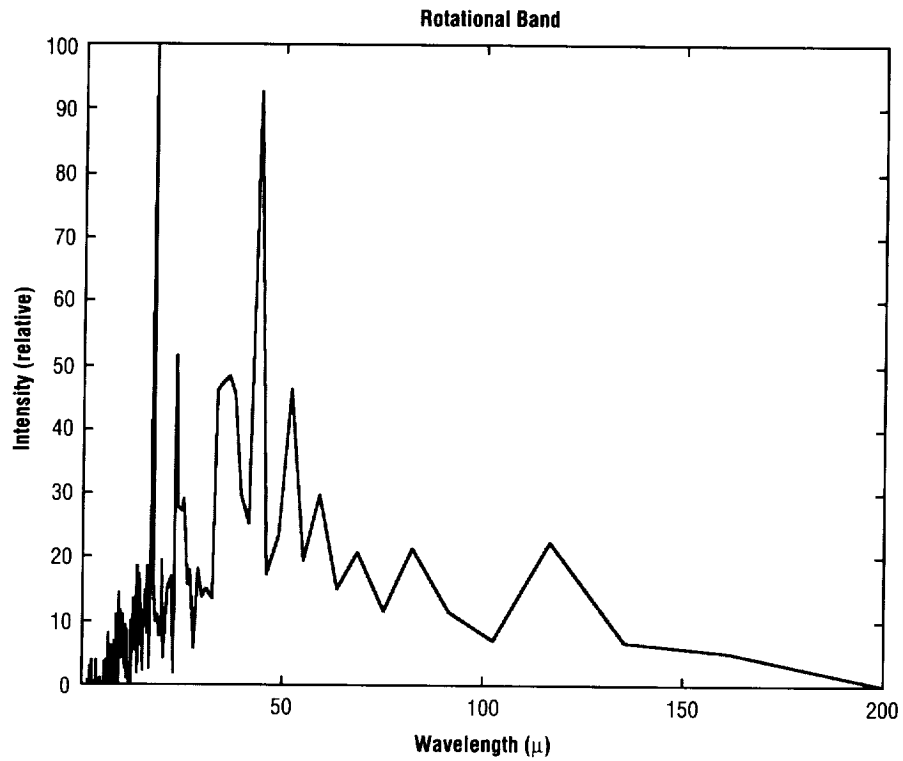
Figure 12. Spectra of H_2O generated by collisional excitation of ≈ 2 eV energy, believed to be excited by ram atmosphere colliding with H_2O which has offgassed from orbiter surfaces but is in the Shuttle atmosphere.
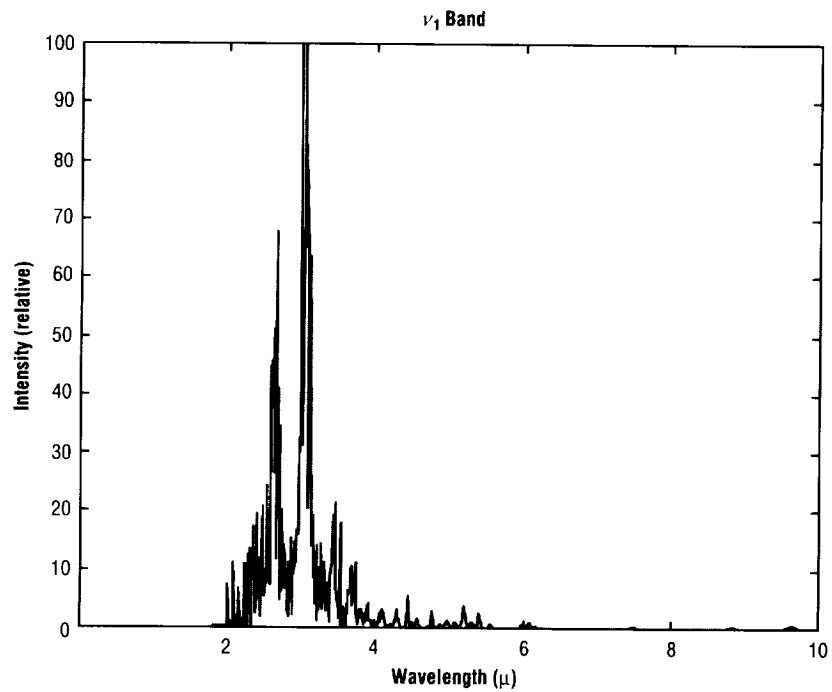
v_1 Band

Figure 13. Same as figure 12 except for the v_1 band of H_2O.
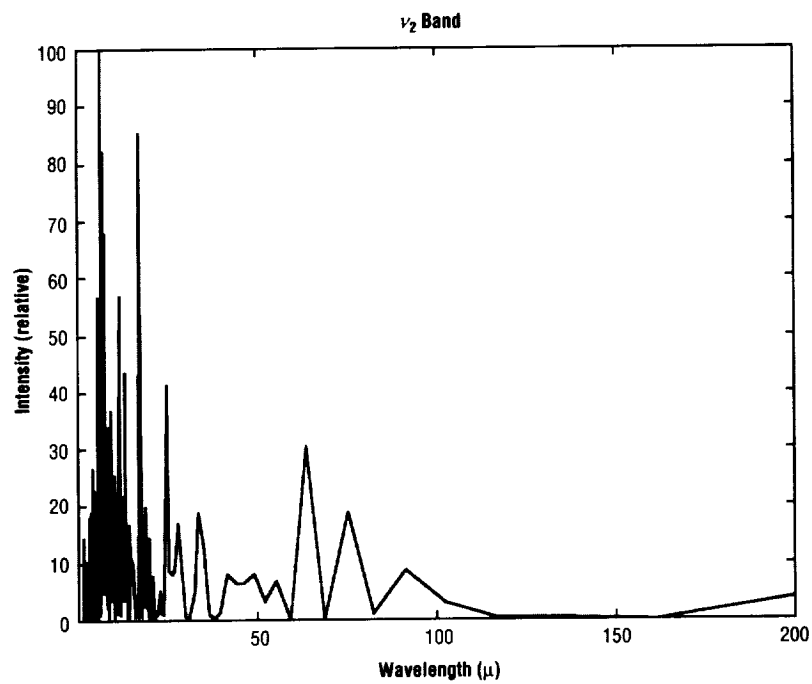
Figure 14.   Same as figure 12 except for the v_2 band of H_2O.
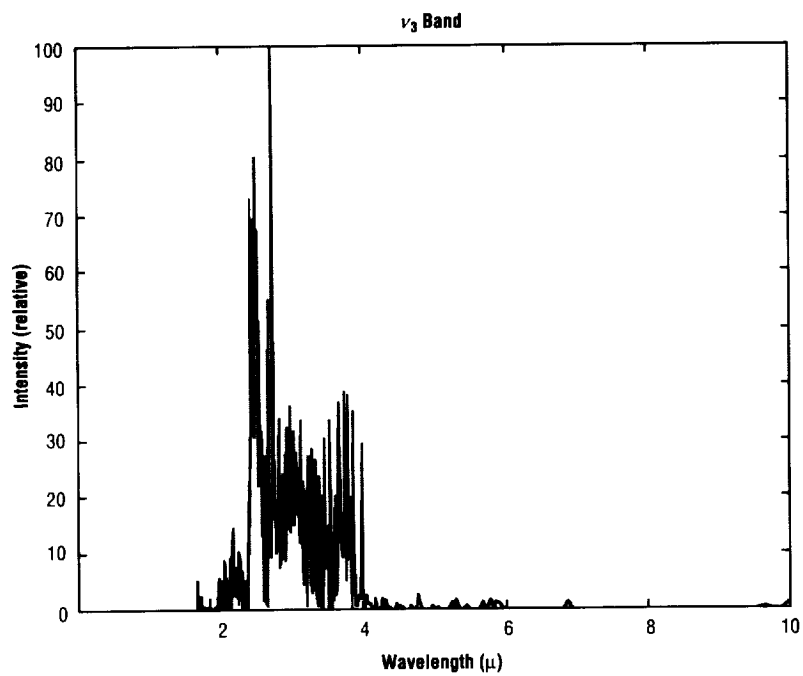
Figure 15.   Same as figure 12 except for the v_3 band of H_2O.

18
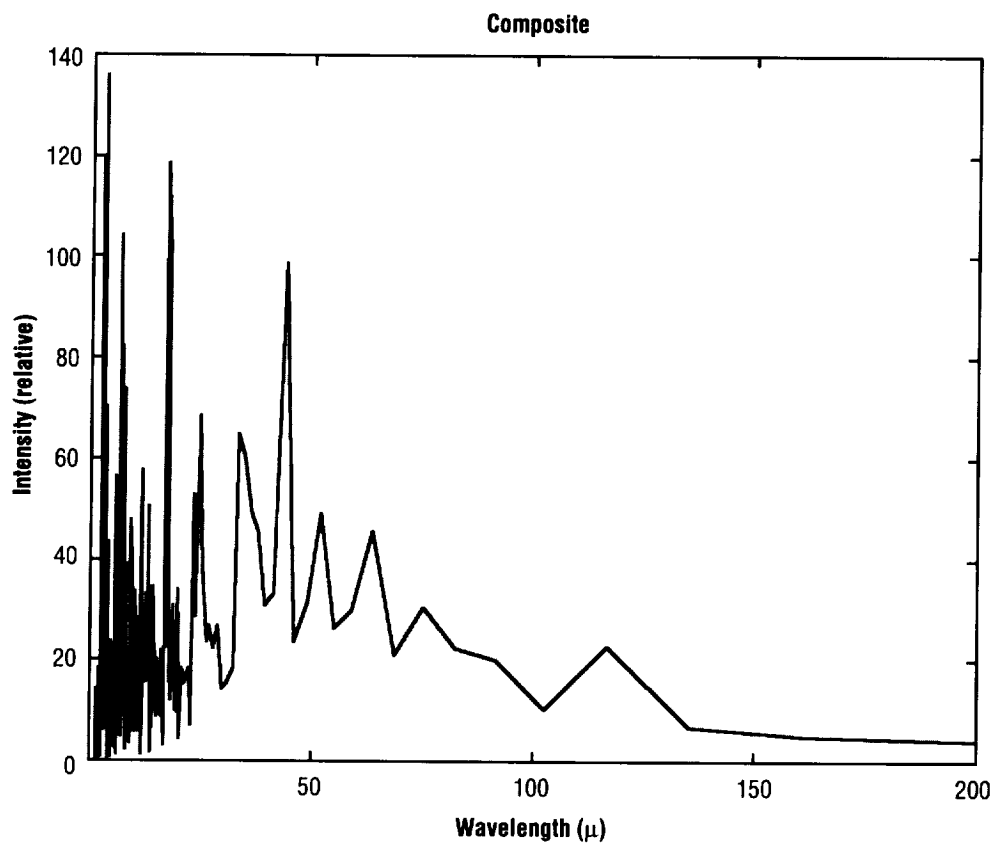
Composite

Figure 16. Same as figure 12 except a composite spectra of H_2O for v_1-v_3 and rotational bands shown in figures 12–15.

5. GLOW MITIGATION

5.1 Visible Wavelength Surface (Heterogeneous) Glows

The heterogeneous (surface stimulated) glows often seen on the vertical stabilizer of the STS are caused by surface-bound NO encountering ram O, forming excited NO_2. The nature of the surfaces which enhance NO to adhere in large numbers are (a) the hygroscopic nature of the surface; i.e., irregular surfaces such as Shuttle tile and carbon paints offer a large surface area for NO to stick; and (b) temperature; i.e., colder surfaces keep more NO on the surface. NO is found naturally in the upper atmosphere which easily provides a saturation source for surfaces. Thruster effluent produces large amounts of NO. When effluent is directed upstream to reencounter surfaces, orbiter surfaces become doped by the orbiter flying through the effluent.

The surface brightness is directly related to the rate at which NO_2^* forms; i.e., linearly with the O fluence, surface-doped NO density, and cross section.

5.1.1 Surface-Doped NO Density

The element least known about is the surface-doped NO density. Since the glows are related to O fluence with altitude, then the NO (which is variable with altitude also) must be at saturation on a given surface for a given temperature. It must be the surface sites of the material that make the physi-bond and NO unite, which is subsequently broken with a ram O recombination. This would suggest further then that porous surfaces are better than nonporous to hold a lot of NO. There is another contributor in orbit to make NO on surfaces from the recombination of N and O on catalytic surfaces (nickel is used in the laboratory for this purpose). It is the fluence of natural NO from the atmosphere that collides and physi-bonds to surfaces. This is the NO source in low-Earth orbit (LEO); however, a catalytic surface such as nickel (Ni) could add more NO through surface catalytics N and O recombinations. These surfaces would not glow any brighter as the NO saturation attribute is what seems to be important.

The next step in this area of research, to establish validation, is to perform some experiments in the laboratory. Leone and Swenson began doing some of these studies at Lockheed in the early 1990's, but a dedicated effort is needed. What comes to mind is to dope surfaces with NO where the surface temperatures are controlled, then bombard those surfaces with an electron beam or, using laboratory methods, study the dopant density versus temperature and material. Until this is done, the only consideration for doping is the assumption that it is only the material temperature which affects the saturation limit of surface bound NO, and consequently the brightness results.

5.1.2 State Change

Does the cross section change for a state change at very low temperatures, where NO goes into an ice state (121 K)? Observations have been made for $T>160$ K (estimated), but suggest that on surfaces <121 K, the NO could layer up as ice, and as such, would have a much reduced cross section for glow.

20

However, this would likely introduce the additional problem in very LEO of NO ice on cryogenic mirrors.

Section 5.1.3 describes some ideas for mitigation. Sections 5.1.3.1 and 5.1.3.5 are the natural, most sensible considerations, based on the observations made to date. Sections 5.1.3.2 and 5.1.3.3 should be followed where possible. Before proceeding with section 5.1.3.4, the laboratory work described above must be addressed.

5.1.3 Mitigation

The following discussion addresses several ideas on how this glow may be eliminated, only from the standpoint of what will eliminate the glow and not from the practicality or necessity of eliminating or reducing it.

5.1.3.1 Glow Brightness. Orbiting at higher altitudes reduces glow linearly with the decrease in O. The O scale height (e folding distance) is $\approx$50 km, thus 50-km higher altitude will reduce the glow brightness by e. In addition, the atmospheric source of NO is reduced. It is not clear from existing measurements that the altitude at which NO no longer saturates the surface continuously is reached, but it is likely between 300–350 km. Above that altitude, glow brightness will be reduced by the product of the decrease in O and atmospheric NO.

5.1.3.2 Gas Releases. The release of inert or nonreactive gases into the upstream (into the velocity vector) interact with the ramming atmospheric O before it reaches orbiter surfaces. This was demonstrated on STS–62, with an N_2 release. It was originally suspected that N_2 + O could result in a significant production of NO at orbit velocities. This was found not to be the case. N_2 is nonreactive with ram O and acts to reduce the O reaching the surface. Consequently, gas releases can reduce glow; although not a practical long-term solution, it certainly is very effective for short periods. A gas density sufficient to chase a ram atom to make a single collision (i.e., a column density of $\approx 10^{15}$ cm^{-2}) before ramming the surface is likely a sufficient density to be highly effective.

5.1.3.3 Thruster Effluent. Monomethyl hydrazine is a type of gas release that produces a large amount of NO. On the Shuttle, some of the thrusters are directed so that a large amount of effluent encounters the surfaces. That effluent is stopped by the surface to form a near-stationary cloud above it, which then can be directed by the momentum exchange of the ram atmosphere to carry the effluent into downstream (away from γ) surfaces. This is frequently seen on the orbiter, where the vernier jets dope the top of the port wing, for example, and the ram atmosphere carries the effluent to become a dopant of bay payloads and Shuttle surfaces. In addition, the NO densities are initially so large in the gas cloud that bright gas phase NO_2 emissions occur. Mitigation here is pretty simple. In future designs, the thrusters should be directed so they do not impinge material back onto surfaces in the thrust. The effluent in the burn will then escape quickly, and only the bright gas phase emission will be visible for a brief time. Optically, it is much better to use a nonthrust system altogether, such as the SKYLAB control moment gyro (CMG) system for attitude control where optical instruments are a major player in the payload. In that design, thrusters were used infrequently to dump momentum from the wheels, but not as the primary attitude control system.

5.1.3.4 Orbiter Surfaces. Nonhygroscopic surfaces are better since, at a given temperature, less real surface area per subtended area is available to hold surface sticking molecules, such as NO. Surfaces such as Shuttle tile and black carbon paints have this trait. This trait in the carbon paints has a very low-reflection coefficient and an isotropic scatterer. Consequently in optical baffles, for instance, the trait is needed for these attributes. This is a speculative issue, and the laboratory experiments described above would be recommended before imposing constraints or guidelines for orbiter surfaces exposed near glow sensitive detectors.

5.1.3.5 Temperature Relationships. Warmer temperatures of surfaces result in lesser NO molecules being bound to the surfaces, and thus not available for heterogeneous processes. This is likely a very practical solution for elimination of baffle glows, for instance, where changing the material is not practical. The temperature relationship for a given material follows closely with $I=I_o\text{EXP}(E/kT)$, where $E=0.14$ eV, k is Boltzman's constant, and T is temperature in Kelvin.

5.2 Infrared, Extended Glows

5.2.1 Background

IR glows observed on the Shuttle are primarily the result of the ram atmosphere interacting with the H_2O vapor outgassing from the Shuttle. Findings suggested that it is the ionospheric O^+ (ions) colliding with H_2O vapor molecules, which resulted in emissions ≈ 2 μ, and that atmospheric O bombarding H_2O vapor was responsible for a broad spectrum ranging from 1–40 μ.

On STS–62, it was also discovered from the IR spectrometer measurements that NO bands were observed in thruster plumes and afterglows. NO is a burn product of the thruster, and thrusters which directly impinge effluent back to Shuttle surfaces cause NO doping and glows.

5.2.2 Mitigation of H_2O Emissions

Section 5.1.3.1 applies slightly in that the O density decreases with altitude, reducing the O fluence to the gas cloud of H_2O. The IR brightness will be directly related to the O fluence, which e-folds every 50 km. Hygroscopic surfaces such as Shuttle tile hold large amounts of H_2O vapor (described in sec. 5.1.3.2). The main mitigation is to keep the orbiter materials dry before launch. The large emissions observed from early Shuttle missions before the Scotchguard™–type treatments have seemingly been very effective. This has been effective in accumulating H_2O before getting into orbit. Also, once in orbit, exposing surfaces to a hot soak will drive the surface-accumulated species off the surfaces more quickly; i.e., as described in sec. 5.1.3.5).

5.2.3 Mitigation of NO Emissions

Thruster-induced NO emissions described in section 5.1.3.3 are believed to be responsible for most NO emissions. Gas phase N produced in burns can readily combine with ram O to form excited NO. Consequently, the burn product emissions cannot be avoided, although the rate of emission is related to the altitude (and the ram O density).

Surface conductors can also lead to a recombination glow in NO, similar to that formed by N and O flows over conductive surfaces such as Ni in laboratory-produced glows and afterglows. Nonconductive surfaces will significantly reduce (or eliminate) this process.

5.3 Ultraviolet and Far-Ultraviolet Glows

5.3.1 Background

Ultraviolet glows in the 200–350 nm region are a result of NO emissions and FUV glows in the 140–200 nm region from N_2 LBH bands. These emissions are primarily sporadic and dominated by thruster dopants. There appear to be UV glows in the 300-nm region, leaving many surface-related astronomy experiments misunderstood.

5.3.2 Mitigation of NO Emissions

5.3.2.1 Thruster Effluent. The dominant glows observed on the Shuttle by the EISG experiment were NO bands in the 200–300 nm spectral region. Nearly all the emission observed was NO in this region (secs. 5.1.3.3 and 5.2). The same mitigation ideas hold for the FUV NO band emissions as did the IR NO band emissions described in section 5.2.

5.3.3 Mitigation of N_2 LBH Bands

The observation of the N_2 LBH bands on STS–62 could not be repeated. Although it was observed in a laboratory experiment prior to flight, the instrument sensitivity may have been too low in the 130–150 nm regime. The LBH bands seen by the Infrared Space Observatory (ISO) experiment on STS–9 were due to surface recombination of N, where N was produced by thruster burns whose effluent came into the Shuttle bay by thruster effluent impinging on Shuttle surfaces and by ram atmosphere upstream from the orbiter momentum exchanging with the effluent. This exchange allows it to slow sufficiently until the Shuttle velocity overtakes the gas. The only mitigation is to eliminate the N sources; i.e., the thruster.

Glows occurring at wavelengths <140 nm have not been addressed here.

REFERENCES

1. Yee, J.-H.; and Abreu, V.J.: "Optical Contamination on the Atmospheric Explorer–E Satellite," *Proc. SPIE Tech. Symp.*, Vol. 338, p. 120, 1982.

2. Yee, J.-H.; and Abreu, V.J.: "Visible Glow Induced by Spacecraft-Environment Interaction," *Geophys. Res. Lett.*, Vol. 10, p. 126, 1983.

3. Yee, J.-H.; and Delgarno, A.: "Radiative Lifetime Analysis of the Spacecraft Optical Glows," *AIAA–83–2660*, AIAA Shuttle Environment and Operations Meeting, p. 191, 1983.

4. Yee, J.-H.; Abreu, V.J.; and Delgarno, A.: "The Atmospheric Explorer Optical Glow Near Perigee Altitudes," *Geophys. Res. Lett.*, Vol. 12, p. 651, 1985.

5. Swenson, G.R.; Mende, S.B.; and Clifton, K.S.: "Ram Vehicle Glow Spectrum; Implication of NO_2 Recombination Continuum," *Geophys. Res. Lett.*, Vol. 12, p. 97, 1985.

6. Swenson, G.R.; Mende, S.B.; and Llewellyn, E.J.: "The Effect of Temperature on Shuttle Glow," *Nature*, Vol. 323, p. 529, 1986.

7. Swenson, G.R.; and Mende, S.B.: "An Analytic Model of Spacecraft Ram Glow Intensities (4000–8000 Å)," *Proc. of the Effect of the Ionosphere on Communication, Navigation, and Surveillance Systems*, Edited by J.M. Goodman, Naval Research Laboratory, May 5–7, 1987.

8. Swenson, G.R.; and Rairden, R.L.: "Spacecraft Glow, Visible Analysis and Modeling, AIAA 34th Aerospace Sciences Meeting, Reno, NV, *AIAA–96–0372*, January 15–18, 1996.

9. Mende, S.B.; Swenson, G.R.; Clifton, K.S.; Gause, R.; Leger, L.; and Garriott, L.K.: Space Vehicle Glow Measurements on STS 41–D, *J. Spacecraft Rock.*, Vol. 23, p. 189, 1986.

10. Swenson, G.R.; Rairden, R.L.; Jennings, D.; and Ahmadjian, M.: "Vehicle Glow Measurements on STS–62," AIAA 33rd Aerospace Sciences Meeting, Reno, NV, *AIAA–95–0491*, January 9–12, 1995.

11. Swenson, G.R.; Rairden, R.L.; Jennings, D.E.; and Ahmadjian, M.: Vehicle Glow Measurements on STS Flight 62, *J. Spacecraft and Rockets*, Vol. 33, pp. 240–249, 1996.

12. Hedin, A.E.: "MSIS–86 Thermospheric Model," *J. Geophys. Res.*, Vol. 92, pp. 4649–4662, 1987.

13. Hunton, D.E., "Thruster Firing Effects in the Shuttle Environment, 1, Neutral Gas Composition," *J. Geophys. Res.*, Vol. 99, pp. 3999–4009, 1994.

14. Viereck, R.A.; Murad, E.; Pike, C.P.; Mende, S.B.; Swenson, G.R.; Elgin, J.B.; Bernstein, L.S.; and Lucid, S.: "O(^{1}D) 630 nm and O(^{1}S) 557.7 nm Emissions in Shuttle Thruster Plumes," *J. Geophys. Res.*, Vol. 100, pp. 5819–5826, 1995.

15. Barrett, J.L.; and Kofsky, I.L.: "The NO–NO$_2$ System at Laboratory Surfaces," Second Workshop on Spacecraft Glow, *NASA Conf. Pub.* #2391, p. 165, 1985.

16. Green, B.D.; Marinelli, W.J.; and Rawlins, W.T.: "Spectral Identification /Elimination of Molecular Species in Spacecraft Glow," Second Workshop on Spacecraft Glow, *NASA Conf. Pub.* #2391, p. 82, May 1985.

17. Kofsky, I.L.; and Barrett, J.L.: "Surface-Catalyzed Recombination Into Excited Electronic, Vibrational, Rotational, and Kinetic Energy States: A Review," Second Workshop on Spacecraft Glow, *NASA Conf. Pub.* #2391, p. 149, May 1985.

18. Kofsky, I.L., "Excitation of N$_2$ LBH Bands Emission by Low Earth-Orbiting Vehicles," *Geophys. Res. Lett.*, Vol. 15, p. 241, 1988.

19. Swenson, G.R.; and Meyerott, R.E.: "Spacecraft Ram Cloud Atom Exhange and N$_2$ LBH Glow," *Geophys. Res. Lett.*, Vol. 15, pp. 245–248, 1988.

20. Meyerott, R.E.; and Swenson, G.R.: "A Surface Chemistry Model for the Production of N$_2$ LBH Spacecraft Glow," *Planetary. Space Sci.*, Vol. 38, pp. 555–566, 1990.

21. Meyerott, R.E.; and Swenson, G.R.: "N$_2$ Spacecraft Glows From N(^{4}S) Recombination," *Planetary Space Sci.*, Vol. 39, 469–478, 1991.

22. Torr, M.R.; and Torr, D.G.: A Preliminary Spectroscopic Assessment of the Spacelab1/Shuttle Optical Environment, *J. Geophys. Res.*, Vol. 90, p. 1683, 1985.

23. Hunton, D.E.; and Machuzak, J.S.: "Thruster Firing Effects in the Shuttle Environment 2, Positive Ion Composition," *J. Geophys. Res.*, Vol. 99, pp. 4011–4022, 1994.

24. Rairden, R.; Swenson, G.R.; Gao, X.; and Finkenor, M.: "UV and FUV Vehicle Glows in Low Earth Orbit," *AICE*, Intersociety Energy Conversion Engineering Conference, Honolulu, HI, pp. 758–763, July 27–August 1, 1997.

25. Upschulte, B.L.; Oakes, D.B.; Caledonia, G.E.; and Blumberg, W.A.M.: "Infrared Emissions Arising From the Reactions of Fast O/O$^+$ With N$_2$," *Geophys. Res. Lett.*, Vol. 19, pp. 993–996, 1992.

26. Herzberg, G.F.R.S.: *Spectra of Diatomic Molecules*, Van Nostrand Reinhold Company, New York, p. 151, 1950.

27. Tanaka, Y.: "Emission Bands of NO in the Vacume Ultraviolet Region Excited in the NO Afterglow," *J. Chem. Phys.*, Vol. 22, No. 12, p. 2047, 1954.

28. Gaydon, A.G.: "The Band Spectrum of NO: The Gamma and Epsilon System," *Proc. Phys. Soc.* (Landon), Vol. 56, p. 95, 1943.

29. Koch, D.G.; Fazio, G.G.; Hoffmann, W.; Melnick, G.; Rieke, G.; Simpson, J.; and Witteborn, F.: "Infrared Observations of Contaminants from Shuttle Flight 51–F," *Adv. Space Res.*, Vol. 7(5), pp. 211–221, 1987.

30. Meyerott, R.E.; Swenson, G.R.; Schweitzer, E.L.; and Koch, D.G.: "Excitation of the Low Lying Vibrational Levels of H_2O by $O(^3P)$ as Measured on Spacelab 2," *J. Geophys. Res.*, Vol. 99, pp. 17,559–17,575, 1994.

31. Briss, E.W.; and Ramsay, D.A.: "Computer Assistance in the Analysis of Molecular Spectra 1. Rotational Structure of High Resolution Singlet-Singlet Bands," *Computer Phys. Commun.*, Vol. 38, pp. 83–112, 1984.

32. Papousek, D.; and Aliev, M.R.: *Molecular Vibrational-Rotational Spectra*, Elsevier Scientific Publishing Company, p. 163, 1982.

33. Redmon, M.J.; and Garrett, B.C.: "Theoretical Studies of Vibrational Excitation in Collisions of $O(^3P)$ with H_2O $(^1A_1),$ " *J. Chem. Phys.*, Vol. 84(2), p. 15, January 1986.

34. Camy-Peyret, C.; and Flaud, J.M.: "The Interacting States (020), (100), and (001) of $H_2{}^{16}O,$ *J. Mole. Spec.*, Vol. 51, pp. 142–150, 1976.

35. Flaud, J.M.; and Camy-Peyret, C.: "The $2v_2$, v_1 and v_3 Bands of $H_2{}^{16}O$ Rotational Study of the (000) and (020) States," *Mole. Phys.*, Vol., 26, No. 4, pp. 811–823, 1973.

REPORT DOCUMENTATION PAGE

Public reporting burden for this collection of information is estimated to average 1 hour per response, including the time for reviewing instructions, searching existing data sources, gathering and maintaining the data needed, and completing and reviewing the collection of information. Send comments regarding this burden estimate or any other aspect of this collection of information, including suggestions for reducing this burden, to Washington Headquarters Services, Directorate for Information Operation and Reports, 1215 Jefferson Davis Highway, Suite 1204, Arlington, VA 22202-4302, and to the Office of Management and Budget, Paperwork Reduction Project (0704-0188), Washington, DC 20503

1. AGENCY USE ONLY (Leave Blank)	2. REPORT DATE October 1999	3. REPORT TYPE AND DATES COVERED Contractor Report (Final)	
4. TITLE AND SUBTITLE Vehicle/Atmosphere Interaction Glows: Far Ultraviolet, Visible, and Infrared		**5. FUNDING NUMBERS** NAS8–40579	
6. AUTHORS G. Swenson			
7. PERFORMING ORGANIZATION NAMES(S) AND ADDRESS(ES) University of Illinois 1308 West Main St. Urbana, IL 61801		**8. PERFORMING ORGANIZATION REPORT NUMBER** M–918	
9. SPONSORING/MONITORING AGENCY NAME(S) AND ADDRESS(ES) George C. Marshall Space Flight Center Marshall Space Flight Center, Alabama 35812		**10. SPONSORING/MONITORING AGENCY REPORT NUMBER** NASA/CR—1999–209254	

11. SUPPLEMENTARY NOTES

Prepared for NASA's Space Environments and Effects (SEE) Program
Technical Monitor: Miria Finckenor

12a. DISTRIBUTION/AVAILABILITY STATEMENT Unclassified-Unlimited Subject Category 92 Standard Distribution	12b. DISTRIBUTION CODE

13. ABSTRACT (Maximum 200 words)

Spacecraft glow information has been gathered from a number of spacecraft including Atmospheric and Dynamic satellites, and Space Shuttles (numerous flights) with dedicated pallet flow observations on STS–39 (DOD) and STS–62 (NASA). In addition, a larger number of laboratory experiments with low energy oxygen beam studies have made important contributions to glow understanding. The following report provides information on three engineering models developed for spacecraft glow including the far ultraviolet to ultraviolet (1400–4000 Å), and infrared (0.9–40 μ) spectral regions. The models include effects resulting from atmospheric density/altitude, spacecraft temperature, spacecraft material, and ram angle. Glow brightness would be predicted as a function of distance from surfaces for all wavelengths.

14. SUBJECT TERMS spacecraft glow, FUV, UV, visible, infrared			15. NUMBER OF PAGES 36
			16. PRICE CODE A03
17. SECURITY CLASSIFICATION OF REPORT Unclassified	18. SECURITY CLASSIFICATION OF THIS PAGE Unclassified	19. SECURITY CLASSIFICATION OF ABSTRACT Unclassified	20. LIMITATION OF ABSTRACT Unlimited

NSN 7540-01-280-5500